VIP Noble-Gas Chemistry Very Important Paper

International Edition: DOI: 10.1002/anie.201606851
German Edition: DOI: 10.1002/ange.201606851

Synthesis and Characterization of $[XeOXe]^{2+}$ in the Adduct-Cation Salt, $[CH_3CN{-}{-}{-}XeOXe{-}{-}{-}NCCH_3][AsF_6]_2$

*John R. DeBackere, Mark R. Bortolus, and Gary J. Schrobilgen**

Dedicated to Professor George A. Olah on the occasion of his 90th birthday

Abstract: *Acetonitrile and [FXeOXe---FXeF][AsF_6] react at −60 °C in anhydrous HF (aHF) to form the CH_3CN adduct of the previously unknown $[XeOXe]^{2+}$ cation. The low-temperature X-ray structure of [CH_3CN---XeOXe---$NCCH_3$][AsF_6]$_2$ exhibits a well-isolated adduct-cation that has among the shortest Xe–N distances obtained for an sp-hybridized nitrogen base adducted to xenon. The Raman spectrum was fully assigned by comparison with the calculated vibrational frequencies and with the aid of ^{18}O-enrichment studies. Natural bond orbital (NBO), atoms in molecules (AIM), electron localization function (ELF), and molecular electrostatic potential surface (MEPS) analyses show that the Xe–O bonds are semi-ionic whereas the Xe–N bonds may be described as strong electrostatic (σ-hole) interactions.*

Although thermodynamically unstable with respect to their elements, oxides of every known xenon oxidation state except $+^1/_2$ have been isolated and characterized in macroscopic quantities.[1] In the case of Xe^{II}, the simplest oxide, XeO, has been observed in the gas-phase by UV and vacuum UV emission spectroscopy where the emission spectrum was attributed to Xe^+O^- ion pair states.[2] Monomeric XeO has only been characterized in an argon matrix by UV spectroscopy which suggested that the ground state is essentially a van der Waals molecule.[3] Subsequent gas-phase quantum-chemical calculations showed XeO to have an unbound $^3\Pi$ ground state with the only bound state being the excited $1^1\Sigma^+$ state.[4]

The first Xe^{II} oxide to be synthesized in isolable amounts was recently reported as a salt of the planar zig-zag shaped $[XeOXeOXe]^{2+}$ cation. The salt, [XeOXeOXe][μ-F-(ReO_2F_3)$_2$]$_2$], was synthesized in aHF at −30 °C by O/F metathesis between ReO_3F and XeF_2 [Eq. (1)] and was characterized by low-temperature single-crystal X-ray diffraction and Raman spectroscopy.[5]

$$4\,ReO_3F \cdot 2\,HF + 3\,XeF_2 \xrightarrow{HF} [XeOXeOXe][\mu\text{-}F(ReO_2F_3)_2]_2 + 2\,[H_3O][HF_2] \quad (1)$$

The related [FXeOXe---FXeF][AsF_6] salt is presently the only known Xe^{II} oxide fluoride.[6] It can be viewed as a fluorine derivative of the $[XeOXe]^{2+}$ cation in which one xenon atom is strongly bound to a terminal fluorine atom and the remaining xenon atom is weakly coordinated to a XeF_2 molecule through a long Xe---F contact.

The reaction of [FXeOXe---FXeF][AsF_6] with excess CH_3CN in HF at −60 °C resulted in the formation of the Xe^{II} oxide cation, $[XeOXe]^{2+}$, as the CH_3CN adduct-cation salt, [CH_3CN—XeOXe—$NCCH_3$][AsF_6]$_2$ [Eq. (2)].

$$2\,[FXeOXe{-}{-}{-}FXeF][AsF_6] + 2\,CH_3CN \xrightarrow{HF} [CH_3CN{-}{-}{-}XeOXe{-}{-}{-}NCCH_3][AsF_6]_2 + XeF_2 + {}^1/_2O_2 + Xe \quad (2)$$

The proposed reaction pathway is described in Scheme S1 of the Supporting Information. As the reaction progressed, crystals of [CH_3CN---XeOXe---$NCCH_3$][AsF_6]$_2$ (space group *C*2/*c*) formed over several hours which proved to be suitable for an X-ray crystal structure determination. The $[CH_3CN{-}{-}{-}XeOXe{-}{-}{-}NCCH_3]^{2+}$ cation (Figure 1 a) lies on a general position (C_1 symmetry). The $[AsF_6]^-$ anions are slightly distorted from O_h symmetry, with two anions located on a C_2-axis and the remaining anion on a general position (Figure S1).

The Xe–O bond lengths (2.032(2), 2.033(2) Å) are well reproduced by gas-phase calculations (2.049 Å) (see Figure 1 and Tables S1 and S2 for a complete list of bond lengths and angles). These values are intermediate with respect to those of the terminal (1.987(6) Å) and central (2.135(6) Å) Xe–O bonds of $[XeOXeOXe]^{2+}$[5] and those of $[FXeOXe{-}{-}{-}FXeF]^+$ (1.938(8) and 2.101(8) Å).[6] The Xe–N distances (2.294(2), 2.304(2) Å) are in excellent agreement with their calculated values (2.306 Å). These bonds are significantly shorter than those of related Xe^{II}–N adducts: [$C_6F_5Xe{-}{-}{-}NCCH_3$][BY_4] (Y = CF_3, 2.640(6); Y = C_6F_5, 2.610(11) Å);[7] [$C_6F_5Xe{-}{-}{-}NCCH_3$][$(C_6F_5)_2BF_2$] (2.681(8) Å);[8] [$C_6F_5Xe{-}{-}{-}NC_5H_3F_2$]-[$AsF_6$] (2.694(5) Å);[9] and [$F_4S$=N-Xe---N≡$SF_3$][$AsF_6$] (2.583(3) Å).[10] In contrast, the Xe–N distances of $[CH_3CN{-}{-}{-}XeOXe{-}{-}{-}NCCH_3]^{2+}$ are very similar to that of [$F_3S{\equiv}N{-}{-}{-}XeF$][$AsF_6$] (2.236(4) Å).[11]

The Xe-O-Xe bond angle (113.0(1)°) of [CH_3CN---XeOXe---$NCCH_3$]$^{2+}$ is similar to those of $[XeOXeOXe]^{2+}$ (115.6(3)°).[5] This angle is substantially less than the calculated gas-phase values of $[CH_3CN{-}{-}{-}XeOXe{-}{-}{-}NCCH_3]^{2+}$ (125.2°) and $[XeOXe]^{2+}$ (123.3°) (Figure S2).

The Xe-N-C angles (Figures 1 and S3) are deformed both in and out of the Xe-O-Xe plane relative to the optimized gas-phase dication (C_{2v}, 175.8°). The angle distortions likely result

[*] J. R. DeBackere, M. R. Bortolus, Prof. G. J. Schrobilgen
Department of Chemistry
McMaster University
Hamilton, ON, L8S 4M1 (Canada)
E-mail: schrobil@mcmaster.ca

Supporting information and the ORCID identification number(s) for the author(s) of this article can be found under http://dx.doi.org/10.1002/anie.201606851.

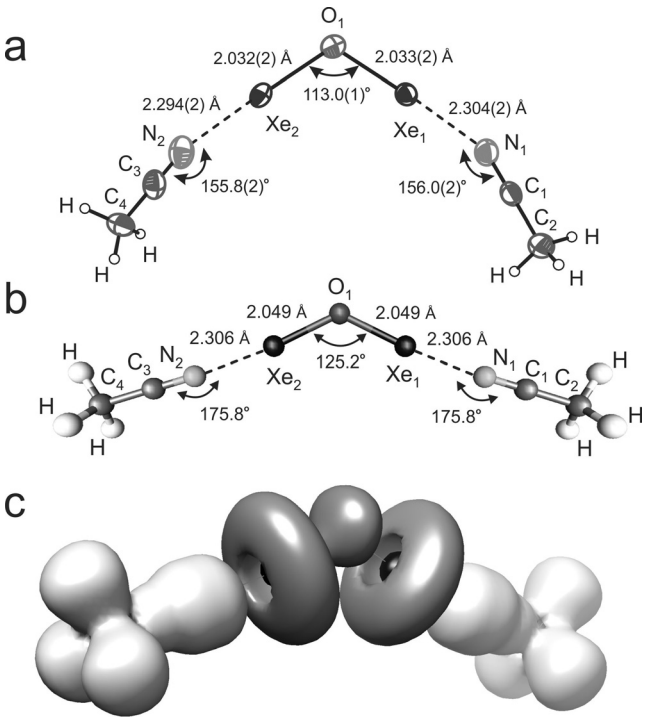

Figure 1. a) The $[CH_3CN{-}{-}{-}XeOXe{-}{-}{-}NCCH_3]^{2+}$ cation in the single-crystal X-ray structure of its $[AsF_6]^-$ salt; thermal ellipsoids are set at 50% probability. b) The energy-minimized gas-phase geometry (C_{2v}) of the $[CH_3CN{-}{-}{-}XeOXe{-}{-}{-}NCCH_3]^{2+}$ cation calculated at the B3LYP/aug-cc-pVTZ(-PP) level of theory, and c) the ELF isosurface plot is shown at $\eta(r) = 0.54$. Black = xenon core basin, dark gray = monosynaptic basins (oxygen and Xe VELP), and light gray = disynaptic basins.

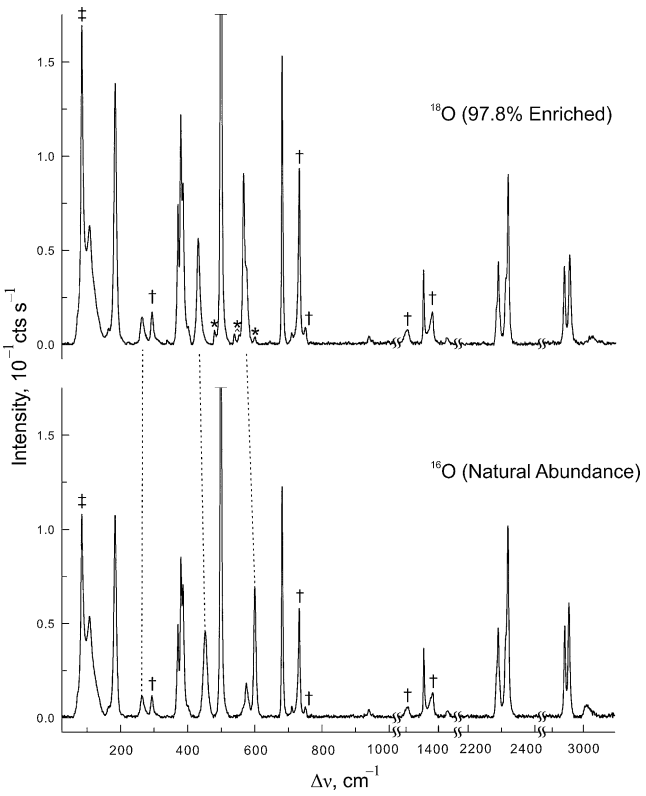

Figure 2. Raman spectra of $[CH_3CN{-}{-}{-}XeOXe{-}{-}{-}NCCH_3][AsF_6]_2$ recorded at −140 °C using 1064-nm excitation for natural abundance (bottom trace) and 97.8% ^{18}O-enriched (top trace) salts. Symbols denote FEP sample tube lines (†), instrumental artifact (∓), and residual $[FXeOXe{-}{-}{-}FXeF][AsF_6]$ (*). The Σ_g^+ band of free XeF_2 (498 cm^{-1}) is the most intense feature in both spectra [see Eq. (2)]. The three vibrational bands of $[XeOXe]^{2+}$ (Table 1) are denoted by dashed lines drawn between the spectra of the ^{16}O- and ^{18}O-isotopologues.

from crystal packing, where long Xe···F cation–anion contacts (3.247(2)–3.563(2) Å) that are close to the sum of the van der Waals radii of xenon and fluorine (3.63 Å)[12] likely contribute to compression of the Xe-O-Xe and Xe-N-C angles and to the torsional angles about the Xe–N bonds.

The Raman spectra of natural abundance and ^{18}O-enriched $[CH_3CN{-}{-}{-}XeOXe{-}{-}{-}NCCH_3][AsF_6]_2$ are shown in Figure 2. Selected experimental and calculated gas-phase frequencies and assignments are provided in Table 1. Full listings of vibrational frequencies and assignments are provided in Table S4.

Vibrational frequencies and isotopic shifts were well reproduced by quantum-chemical calculations. Bands associated with $[AsF_6]^-$ were assigned by comparison with their previously published frequencies.[6] In the ensuing discussion, the Raman frequencies of the ^{18}O-enriched compounds are given in square brackets following their natural abundance ^{16}O-values. In accordance with adduct formation, high-

Table 1: Selected Raman frequencies, $^{16/18}O$ isotopic shifts, and assignments for the $[CH_3CN{-}{-}{-}XeOXe{-}{-}{-}NCCH_3]^{2+}$ cation and isolated $[XeOXe]^{2+}$ cation.[a]

Experimental[b]			Calculated[b,c]			Assignment
^{16}O	^{18}O	$\Delta\nu^{16/18}$	^{16}O	^{18}O	$\Delta\nu^{16/18}$	
$[CH_3CN{-}{-}{-}XeOXe{-}{-}{-}NCCH_3]^{2+}$						
599.9(100)	566.4(100)	−33.5	586.0(32)	554.9(29)	−31.1	$\nu(Xe_1O)-\nu(Xe_2O)$
452.0(66)	431.0(62)	−21.0	443.8(34)	428.6(15)	−15.2	$\nu(Xe_1O)+\nu(Xe_2O)+[(\delta(CCN)_{A+B})_{ip}]_{small}$
263.9(15)	263.7(16)	−0.2	243.0(15)	243.1(16)	0.1	$\delta(Xe_1OXe_2)_{ip}-\nu(XeN)_{A+B}$
$[XeOXe]^{2+}$						
			505.4(4)	479.0(3)	−26.4	$\nu(Xe_1O)-\nu(Xe_2O)$
			424.6(8)	404.1(7)	−20.5	$\nu(Xe_1O)+\nu(Xe_2O)$
			123.9(11)	124.6(11)	−0.7	$\delta(Xe_1OXe_2)_{ip}$

[a] A complete list of vibrational frequencies and their assignments is provided in Tables S3 and S4; abbreviations are defined in their footnotes. [b] Vibrational frequencies and $^{16/18}O$-isotopic shifts [$\Delta\nu^{16/18} = \nu(^{18}O)-\nu(^{16}O)$] are given in cm^{-1} and experimental relative intensities and calculated intensities (Å amu^{-1}) are given in parentheses. The atom labeling scheme is given in Figures 1 and S2. [c] B3LYP/aug-cc-pVTZ(-PP) level of theory.

frequency ligand complexation shifts relative to free CH_3CN[13] occur for ν(CN) (Δν(CN), 36 and 42 cm^{-1}) and ν(CC) (Δν(CC), 19 cm^{-1}).

The asymmetric Xe–O stretching mode, $\nu(Xe_1O)-\nu(Xe_2O)$, occurs at 599.9 [566.4] cm^{-1} and is well reproduced by the calculated value, 586.0 [554.9] cm^{-1}. The experimental (−33.5 cm^{-1}) and calculated (−31.1 cm^{-1}) isotope shifts, $\Delta\nu^{16/18}$, are in excellent agreement. This frequency is comparable to that of the symmetric out-of-phase stretching mode (ν_1, A_g) of the $[XeOXeOXe]^{2+}$ cation, which occurs at 581.6 [549.3] cm^{-1} and possesses a similar $^{16/18}O$ isotope shift (−32.3 cm^{-1}).[5]

The symmetric stretching mode, $\nu(Xe_1O)+\nu(Xe_2O)$, is weakly coupled to the $\delta(CCN)_{ip}$ deformation modes of the CH_3CN ligands. The band occurs at 452.0 [431.0] cm^{-1} which is well reproduced by the calculated values (443.8 [428.6] cm^{-1}). The experimental (−21.0 cm^{-1}) and calculated (−15.2 cm^{-1}) $^{16/18}O$ isotope shifts are in good agreement but are much smaller in magnitude than those of the asymmetric stretching mode. The $^{16/18}O$ isotope shift of the in-phase symmetric stretching mode (ν_2, A_g) of $[XeOXeOXe]^{2+}$ (exptl, −17.8 cm^{-1}; calcd, −18.9 cm^{-1}) is comparable to that of the adducted $[XeOXe]^{2+}$ cation. However, the symmetric stretching frequency of $[CH_3CN{-}{-}{-}XeOXe{-}{-}{-}NCCH_3]^{2+}$ is considerably higher than the experimental value of $[XeOXeOXe]^{2+}$ (358.7 [340.9] cm^{-1}). The calculated gas-phase frequency of $[XeOXe]^{2+}$ (424.6 [404.1] cm^{-1}) is only slightly shifted to lower frequency relative to that of the CH_3CN adduct-cation, suggesting that coupling with CH_3CN has a relatively small effect on the observed frequency. The band at 263.9 [263.7] cm^{-1} is assigned to the $\delta(Xe_1OXe_2)_{ip}$ bending mode which is strongly coupled with the in-phase xenon-nitrogen stretching mode, $\nu(XeN)_{A+B}$. The calculated frequency (243.0 [243.1] cm^{-1}) is in good agreement with the experimental value and also does not exhibit an $^{16/18}O$ isotope shift. The corresponding bending mode of $[XeOXeOXe]^{2+}$ also did not exhibit an isotope shift.[5] The $\delta(Xe_1OXe_2)_{ip}$ bend of $[CH_3CN{-}{-}{-}XeOXe{-}{-}{-}NCCH_3]^{2+}$ occurs at a much higher frequency than that of $[XeOXeOXe]^{2+}$ (92.8 [90.3] cm^{-1}), highlighting the effect of strong coupling with the Xe–N stretching modes. This interpretation is supported by the calculated gas-phase $\delta(Xe_1OXe_2)_{ip}$ bending frequencies of $[XeOXe]^{2+}$ (123.9 [124.6] cm^{-1}), which occur at significantly lower frequencies than its CH_3CN adduct.

The NBO analysis[14] (Table S5) shows that the O and Xe atom charges of $[CH_3CN{-}{-}{-}XeOXe{-}{-}{-}NCCH_3]^{2+}$ (O, −0.865; Xe, +1.190) and $[XeOXe]^{2+}$ (O, −0.575; Xe, +1.288) are considerably less than the formal charges expected for a purely ionic compound (O, −2; Xe, +2) and are consistent with semi-ionic bonding. The greater charge difference between Xe and O in $[CH_3CN{-}{-}{-}XeOXe{-}{-}{-}NCCH_3]^{2+}$ (2.055) relative to that of $[XeOXe]^{2+}$ (1.863) also suggests slightly more ionic Xe−O bonds in the adduct-cation. Furthermore, there is significant negative charge transfer from the CH_3CN ligands onto the $[XeOXe]^{2+}$ cation, resulting in an overall +1.515 charge on the XeOXe-moiety and +0.242 charge on each CH_3CN ligand. Charge transfer results in Xe−N (0.330) and Xe−O (0.676) Wiberg bond indices that are significantly smaller than those of the gas-phase $[XeOXe]^{2+}$ cation (0.929). The NLMO analysis (Table S6) also shows that the nitrogen valence electron lone pair (VELP) of CH_3CN is mostly localized (86.1%) in an sp-hybridized orbital (s, 50.3%; p, 49.6%) with 12.9% delocalized into the $\sigma^*_{Xe\text{-}O}$ LUMO which is primarily p in character (Xe: 1.1% s, 98.4% p; O: 8.8% s, 90.6% p). The second-order perturbation analysis shows each $n_N \rightarrow \sigma^*_{Xe\text{-}O}$ interaction contributes 208.1 kJ mol^{-1} of stabilization.

The gas-phase binding energies (B3LYP level) were also calculated for the Xe–N interactions. Coordination of a single CH_3CN ligand [Eq. (3)] to $[XeOXe]^{2+}$ gave a larger energy change than coordination of a second CH_3CN ligand [Eq. (4)].

$$[XeOXe]^{2+} + CH_3CN \rightarrow [CH_3CN{-}{-}{-}XeOXe]^{2+} \quad -454.0\ kJ\ mol^{-1} \tag{3}$$

$$[CH_3CN{-}{-}{-}XeOXe]^{2+} + CH_3CN \rightarrow [CH_3CN{-}{-}{-}XeOXe{-}{-}{-}NCCH_3]^{2+} \quad -329.6\ kJ\ mol^{-1} \tag{4}$$

These binding energies are substantially greater than those calculated for $F_6XeNCCH_3$ (−157.1 kJ mol^{-1}) and $F_6Xe(NCCH_3)_2$ (−129.5 kJ mol^{-1}) at the MP2 level.[15] Although different levels of theory do not allow a precise comparison to be made, it is apparent that $[XeOXe]^{2+}$ is a much stronger Lewis acid toward CH_3CN than XeF_6.

Computational studies were carried out to assess the nature of bonding by use of QTAIM,[16] MEPS, and ELF analyses.[17,18] The details of these analyses are provided in the Supporting Information. The topologies of the electron localization domains are depicted in Figure 1c. Among the prominent features of the ELF isosurface plots are the toroidal-shaped Xe valence electron densities resulting from the combination of the three nonbonding VELP domains with the exposed Xe core basins at their centers. The exposed core region maxima of +1126 kJ mol^{-1} on the Xe atoms in the MEPS of $[XeOXe]^{2+}$ (Figure S4) correspond to σ-holes into which the N VELPs coordinate. The MEPS of $[XeOXe]^{2+}$ also show that the minimum electrostatic potential (EP), +849 kJ mol^{-1}, resides on the oxygen atom. These EPs are considerably more positive than the corresponding maximum and minimum of $[XeOXeOXe]^{2+}$ (+895 and +635 kJ mol^{-1}).[5] The MEPs also show EP maxima between the Xe atoms of $[XeOXe]^{2+}$ (+1116 kJ mol^{-1}) and the adduct-cation (+818 kJ mol^{-1}) and EP minima on the O atoms (+849 and +533 kJ mol^{-1}, respectively). The O atom and inter-Xe atom EPs both decrease by about +300 kJ mol^{-1} upon adduct formation, indicative of significant negative charge transfer onto the cation. Polarization of the N VELPs by the Xe σ-holes is in accordance with the description provided by the NBO analysis relating to delocalization of the N VELP into the $\sigma^*_{Xe\text{-}O}$ LUMO. The relative strength of the σ-hole interaction is also reflected in the ELF reduction of localization diagram (Figure S8) which shows that the adduct separates ($f_{sep}=0.32$) into $[XeOXe]^{2+}$ and two CH_3CN molecules at a significantly greater separation value than the Xe core basins ($f_{sep}=0.22$), approaching those of the semi-ionic Xe−O bonds ($f_{sep}=0.44$). This is consistent with a relatively strong Xe−N bonding interaction. In contrast,

the Xe^{VI} adducts, $F_6XeNCCH_3$ and $F_6Xe(NCCH_3)_2$, separate into CH_3CN and XeF_6 *f*-localization domains significantly before the separation of the Xe core basin which is indicative of considerably weaker Xe–N bonding interactions.[19]

Experimental Section

In a typical synthesis, the starting material, $[FXeOXeFXeF][AsF_6]$, was prepared from $[H_3O][AsF_6]$ (0.124 g, 0.597 mmol) and XeF_2 (0.118 g, 0.611 mmol) in aHF solvent (ca. 0.5 to 0.7 mL) in a T-shaped $^1/_4$-in. o.d. FEP reaction vessel equipped with a Kel-F valve as previously described.[6] Dry CH_3CN (ca. 0.2 mL) was then condensed under static vacuum at −196 °C onto the frozen $[FXeOXeFXeF][AsF_6]$ and HF mixture. The reaction mixture was warmed to −78 °C to allow HF to melt and dissolve CH_3CN. After 2 h at −78 °C, the mixture was warmed to −60 °C for 2 h over which time slow gas evolution occurred and pale yellow crystals formed as the starting material dissolved and reacted. The reaction mixture was then cooled to −78 °C for 12 h and the supernatant was decanted into the side arm of the reactor and heat sealed off, leaving behind pale yellow plate-shaped crystals that were wetted with HF. The low-temperature Raman spectra (−140 °C) were obtained on the wetted crystalline compound (Figure 2) as previously described.[20] A crystal was mounted on a X-ray diffractometer using a modification of a previously described low-temperature crystal mounting technique.[20] X-ray diffraction data were collected at −173 °C; space group $C2/c$, $a = 23.8785(8)$, $b = 11.4645(4)$, $c = 12.5440(4)$ Å, $\beta = 109.064(2)°$, $Z = 8$, $V = 3245.64$ Å^3 and refined to $R_1 = 0.0292$ and $wR_2 = 0.0714$ (also see Supporting Information, Table S7). Details relating to synthetic work, Raman spectroscopy, low-temperature crystal mounting, X-ray data collection, and X-ray structure refinement are provided in the Supporting Information.

CCDC 1496589 contains the supplementary crystallographic data for this paper. These data can be obtained free of charge from The Cambridge Crystallographic Data Centre.

Acknowledgements

We thank the Natural Sciences and Engineering Research Council (NSERC) of Canada for financial support in the form of a Discovery Grant (G.J.S.) and a CGS-D Scholarship (J.R.D.), and SHARCNet (Shared Hierarchical Academic Research Computing Network; http://www.sharcnet.ca) for providing computational resources. We also thank Dr. Hélène P.A. Mercier, McMaster University, for her guidance relating to AIM and ELF calculations, and for her valued critique of this manuscript.

Keywords: fluorine chemistry · noble-gas chemistry · xenon(II) oxides · xenon–nitrogen bonds · σ-hole bonding

How to cite: *Angew. Chem. Int. Ed.* **2016**, *55*, 11917–11920
Angew. Chem. **2016**, *128*, 12096–12099

[1] a) D. S. Brock, G. J. Schrobilgen, *J. Am. Chem. Soc.* **2011**, *133*, 6265–6269; b) D. F. Smith, *J. Am. Chem. Soc.* **1963**, *85*, 816–817; c) D. H. Templeton, A. Zalkin, J. D. Forrester, S. M. Williamson, *J. Am. Chem. Soc.* **1963**, *85*, 817; d) W. C. Hamilton, J. A. Ibers, D. R. Mackenzie, *Science* **1963**, *141*, 532–534; e) H. Selig, H. H. Claassen, C. L. Chernick, J. G. Malm, J. L. Huston, *Science* **1964**, *143*, 1322–1323; f) M. Gerken, G. J. Schrobilgen, *Inorg. Chem.* **2002**, *41*, 198–204, and references therein; g) T. Vent-Schmidt, J. T. Goettel, G. J. Schrobilgen, S. Riedel, *Chem. Eur. J.* **2015**, *21*, 11244–11252.
[2] a) M. F. Golde, B. A. Trush, *Chem. Phys. Lett.* **1974**, *29*, 486–490; b) J. Xu, D. W. Setser, J. K. Ku, *Chem. Phys. Lett.* **1986**, *132*, 427–436; c) A. Kvaran, A. Ludviksson, W. S. Hartree, J. P. Simons, *Chem. Phys. Lett.* **1987**, *137*, 209–218; d) D. E. Johnson, *Chem. Phys. Lett.* **1995**, *238*, 71–76.
[3] B. S. Ault, L. Andrews, *Chem. Phys. Lett.* **1976**, *43*, 350–352.
[4] a) T. H. Dunning, P. J. Hay, *J. Chem. Phys.* **1977**, *66*, 3767–3777; b) S. R. Langhoff, *J. Chem. Phys.* **1980**, *73*, 2379–2386; c) M. Yamanishi, K. Hirao, K. J. Yamashita, *J. Chem. Phys.* **1998**, *108*, 1514–1521.
[5] M. V. Ivanova, H. P. A. Mercier, G. J. Schrobilgen, *J. Am. Chem. Soc.* **2015**, *137*, 13398–13413.
[6] M. Gerken, M. D. Moran, H. P. A. Mercier, B. E. Pointner, G. J. Schrobilgen, B. Hoge, K. O. Christe, J. A. Boatz, *J. Am. Chem. Soc.* **2009**, *131*, 13474–13489.
[7] K. Koppe, H. J. Frohn, H. P. A. Mercier, G. J. Schrobilgen, *Inorg. Chem.* **2008**, *47*, 3205–3217.
[8] H. J. Frohn, S. Jakobs, G. Henkel, *Angew. Chem. Int. Ed. Engl.* **1989**, *28*, 1506–1507; *Angew. Chem.* **1989**, *101*, 1534–1536.
[9] H. J. Frohn, T. Schroer, G. Henkel, *Z. Naturforsch. B* **1995**, *50*, 1799–1810.
[10] G. L. Smith, G. J. Schrobilgen, *Inorg. Chem.* **2009**, *48*, 7714–7728.
[11] G. L. Smith, H. P. A. Mercier, G. J. Schrobilgen, *Inorg. Chem.* **2007**, *46*, 1369–1378.
[12] A. Bondi, *J. Phys. Chem.* **1964**, *68*, 441–451.
[13] D. S. Brock, V. Bilir, H. P. A. Mercier, G. J. Schrobilgen, *J. Am. Chem. Soc.* **2007**, *129*, 3598–3611.
[14] NBO 6.0. E. D. Glendening, J. K. Badenhoop, A. E. Reed, J. E. Carpenter, J. A. Bohmann, C. M. Morales, C. R. Landis, F. Weinhold, Theoretical Chemistry Institute, University of Wisconsin, Madison, **2013**.
[15] K. Matsumoto, J. Haner, H. P. A. Mercier, G. J. Schrobilgen, *Angew. Chem. Int. Ed.* **2015**, *54*, 14169–14173; *Angew. Chem.* **2015**, *127*, 14375–14379.
[16] R. F. W. Bader in *Atoms in Molecules: A Quantum Theory*, Oxford University Press, Oxford, **1990**.
[17] B. Silvi, A. Savin, *Nature* **1994**, *371*, 683–686.
[18] A. D. Becke, K. E. Edgecombe, *J. Chem. Phys.* **1990**, *92*, 5397–5403.
[19] J. Haner, K. Matsumoto, H. P. A. Mercier, G. J. Schrobilgen, *Chem. Eur. J.* **2016**, *22*, 4833–4842.
[20] M. Gerken, D. A. Dixon, G. J. Schrobilgen, *Inorg. Chem.* **2000**, *39*, 4244–4255.

Received: July 14, 2016
Published online: August 25, 2016

